Int J Energy Environ Eng (2016) 7:273–287
DOI 10.1007/s40095-016-0214-4

ORIGINAL RESEARCH

Hydrodeoxygenation of cracked vegetable oil using $CoMo/Al_2O_3$ and Pt/C catalysts

Emanuel Baldauf[1] · Anika Sievers[1] · Thomas Willner[1]

Received: 21 November 2015 / Accepted: 30 June 2016 / Published online: 9 July 2016

Abstract During the continuous catalytic hydrodeoxygenation (HDO) of cracked vegetable oil (CVO), CO_2 and CO occur as the main reaction gases, in addition to hydrocarbon gases such as CH_4 and C_2H_6. The catalysts used were cobalt-molybdenum (CoMo) on an Al_2O_3 support and platinum (Pt) on an active carbon. All named gas components can result directly from the decomposition of CVO. The results of batch experiments for gas phase reactions (GPRs) under the same 50 bar H_2 atmosphere using the same catalysts (CoMo, Pt) indicate that CO and CH_4 can also be formed by GPRs. CO can result from the reverse water–gas shift reaction (RWGS), and CH_4 from CO- or CO_2-methanation. The found CO-yields from GPRs are within the theoretical thermodynamic limits based on equilibrium. An unexpected inhomogeneity of the gas component concentrations in the reactor during batch investigations was observed despite the elevated temperature (380 °C) and high RPM (1100) due to the high density difference compared to H_2, especially in the case of CO_2.

Keywords Catalytic hydrodeoxygenation · Cracked vegetable oil · Biofuel · Gas residence time · Gas phase reactions · Gas phase inhomogeneity

Abbreviations

HDO	Hydrodeoxygenation
CVO	Cracked vegetable oil
CoMo	Cobalt molybdenum
Pt	Platinum
GPRs	Gas phase reactions
RWGS	Reverse water–gas shift reaction
DO	Deoxygenation
DEC	Decarboxylation/decarbonylation
HYD	Hydrogenation

✉ Emanuel Baldauf
emanuel.baldauf@gmail.com

[1] Department Process Engineering, Faculty of Life Sciences, Hamburg University of Applied Sciences, Ulmenliet 20, 21033 Hamburg, Germany

Introduction

The rapid growth of world's population and rising desire for prosperity are driving the demand for energy and transportation fuels. According to the IEA scenarios [1, 2], this goes along with increasing importance of biofuels. To overcome limitations in blending potential of biofuels, drop-in quality is favourable. One established pathway in this direction is the production of hydroprocessed vegetable oil [3].

A comparable approach is a two-step upgrading of vegetable oils via thermal deoxygenation (DO) in the first step producing CVO and subsequent hydroprocessing to obtain hydroprocessed CVO [4, 5]. The CVO production step was investigated in detail before; during this step, a decrease of the vegetable oils' initial oxygen content (approximately 10 wt %) to 5 wt % was reached [4, 6]. It was shown that the CVO's oxygen is mainly (87 wt %) bound in free fatty acids [5]. Batch studies on HDO of CVO gave the first indications of catalytic influences on oxygen and energy content of hydroprocessed CVO [5]. Semi-continuous studies were performed to approach suitable feed rates (CVO, H_2) for the continuous HDO of CVO [7]. Optimal reaction conditions for all investigations of this work were found to be 380 °C, 50 bar H_2 pressure and a gas entrainment impeller rotation speed of 1100 RPM [5, 7].

DO and HDO of fatty acids is widely discussed in literature [8–15]. HDO implies the direct participation of H_2 in a reaction, while DO in general does not necessarily require H_2. According to the aforementioned literature, the main gaseous products from DO/HDO of fatty acids are CO_2 from decarboxylation and CO from decarbonylation reactions for both DO and HDO, while reaction water may result from at least three pathways: first, along with decarbonylation; second, from dehydration (during DO/HDO) and third, via hydrogenation (reduction) in case of HDO. Further gaseous products may be short-chain hydrocarbons such as CH_4 and C_2H_6. One possibility for the formation of hydrocarbon gases is cracking [8, 16]. CH_4 can also result from GPRs such as methanation of CO and CO_2. Furthermore, CO can also result from CO_2 and H_2 via RWGS. These GPRs as shown in Eqs. (1–3) are reported by Gusmão et al. [12], Wagman et al. [17], Snåre et al. [18], Lestari et al. [19] and Madsen et al. [11].

The present work focuses on three main questions: Which are the main gaseous and liquid products occurring during HDO of CVO? Which interrelationship between gas and liquid-phase composition can be identified? Which GPRs can take place in parallel of HDO of CVO? Based on these questions, the objective of this work is to study the influence of two different catalysts: A typical hydrotreatment catalyst $CoMo/Al_2O_3$ and Pt/C as a noble metal catalyst [20]. For the HDO investigations of CVO, continuous experiments are performed. GPRs are studied using a batch configuration of the setup to allow an overall mass balance of the experiments. Thermodynamics of GPRs are worked out to support the findings from the experimental work.

Thermodynamic section of GPRs

The thermodynamic section shall give some insights regarding Gibbs free energy and reaction equilibrium data for the considered GPRs. The main gaseous products observed during HDO of CVO are CO_2, CO and CH_4. According to the literature mentioned above, RWGS and methanation of CO and CO_2 are the expected GPRs under H_2 atmosphere (1–3).

$$CO_2 + H_2 \overset{T,p}{\leftrightarrow} CO + H_2O, \tag{1}$$

$$CO + 3H_2 \overset{T,p}{\leftrightarrow} CH_4 + H_2O, \tag{2}$$

$$CO_2 + 4H_2 \overset{T,p}{\leftrightarrow} CH_4 + 2H_2O. \tag{3}$$

Equation (3) may be represented by the combination of Eqs. (1) and (2). Therefore, reactions (1, 2) will be mainly considered in the following. To compare experimental results with thermodynamic equilibrium, data for reactions (1, 2) were calculated for the applied reaction temperature. First, it was proved if the GPRs are exergonic or endergonic (Eq. 4). The calculation of reaction enthalpy and reaction entropy according to (5, 6) is carried out with data from Basu [21] and National Institute of Standards and Technology [22].

$$\Delta G_R = \Delta H_R - T \times \Delta S_R, \tag{4}$$

$$\Delta H_R(T) = \Delta H_R(T_0) + \sum \nu_i \cdot \left[a_i \cdot (T - T_0) + \frac{b_i}{2} \cdot \left(T^2 - T_0^2\right) + \frac{c_i}{3} \cdot \left(T^3 - T_0^3\right) + \frac{d_i}{4} \cdot \left(T^4 - T_0^4\right) \right], \tag{5}$$

$$\Delta S_R(T) = \Delta S_R(T_0) + \sum \nu_i \cdot \left[a_i \cdot \ln\left(\frac{T}{T_0}\right) + b_i \cdot (T - T_0) + \frac{c_i}{2} \cdot (T^2 - T_0^2) + \frac{d_i}{3} \cdot (T^3 - T_0^3) \right], \tag{6}$$

where ΔG_R Gibbs free energy (kJ/mol), ΔH_R reaction enthalpy (kJ/mol), T temperature (K), ΔS_R reaction entropy (kJ/mol K), $\Delta H_R(T_0)$ reaction enthalpy at T_0 (1 bar) using data from National Institute of Standards and Technology [22] (kJ/mol), T_0 reference temperature (298.15 K) (K), ν_i stoichiometric factor of component i, $a_i \ldots d_i$ coefficients of component i according to Basu [21] (kJ/mol), $\Delta S_R(T_0)$ reaction entropy at T_0 (1 bar) using data from National Institute of Standards and Technology [22] (kJ/mol K).

It was found that the RWGS is endergonic in the considered temperature range, whereas CO-methanation is exergonic, as can be seen from Gibbs free energy for each reaction. Detailed results are shown in Table 1.

These values are in good agreement with the literature data from Snåre, et al. [18] which provided data for the reaction enthalpy and Gibbs free energy for reactions (1) and (2) at 573.15 K ($\Delta H_{R,(1)} = 39.2$ kJ/mol, $\Delta H_{R,(2)} = -216.4$ kJ/mol, $\Delta G_{R,(1)} = 17.6$ kJ/mol, $\Delta G_{R,(2)} = -78.7$ kJ/mol).

Due to these thermodynamic results, a low equilibrium constant ($K_{p,(1)}$) is expected for RWGS, while equilibrium

Table 1 Calculated reaction enthalpy ΔH_R, reaction entropy ΔS_R and Gibbs free energy ΔG_R for GPRs according to Eqs. (1, 2) depending on temperature at 1 bar

	T (K)	Reaction, equation		
		RWGS, (1)	CO-Methanation, (2)	
$\Delta H_R\ (T_0)$	298.15	41.1	−206.2	kJ/mol
ΔH_R	573.15	39.3	−216.8	kJ/mol
ΔH_R	653.15	38.5	−219.0	kJ/mol
$\Delta S_R\ (T_0)$	298.15	0.042	−0.215	kJ/mol K
$\Delta G_R\ (T_0)$	298.15	28.6	−142.2	kJ/mol
ΔG_R	573.15	17.6	−79.0	kJ/mol
ΔG_R	653.15	14.6	−59.6	kJ/mol

constant for CO-methanation should be high. The thermodynamic equilibrium constant for the RWGS reaction (1) and CO-methanation (2) are calculated according to Eq. (7) based on the data from Elvers [23].

$$K_p = 10^{\left(a+\frac{b}{T}+c\cdot\log(T)+d\cdot T+e\cdot T^2\right)}, \quad (7)$$

where K_p equilibrium constant, $a\ldots e$ coefficients according to Elvers [23], T temperature in K.

Accordingly, the equilibrium constants for RWGS (1) and CO-methanation (2) were calculated. Equilibrium constants are 0.070 for RWGS (1) and 6×10^4 bar^{-2} for CO-methanation (2) (at 380 °C, 1 bar).

Experimental section

Materials

Two different catalysts were used: molybdenum with cobalt traces on an Al_2O_3 support ($CoMo/Al_2O_3$; BET surface area = 140 m^2/g; 20 wt % MoO_3, 5 wt % CoO; 9.4 nm mean pore diameter; 0.34 mL/g pore volume) and platinum on a carbon support (Pt/C; BET surface area = 650 m^2/g; 5 wt % Pt; 2.4 nm mean pore diameter; 0.39 mL/g pore volume). Both catalysts were provided by Clariant International, Ltd. (Muttenz, Switzerland). Calibration gases (N4, N21, Crystal-mixtures) and H_2 (purity > 99.999 mol %) were purchased from Air Liquide (Hamburg, Germany). Pt and CoMo catalysts for HDO purposes were applied and have already been widely studied [5, 24–28]. The CoMo catalyst was provided string-shaped in a basket, and the Pt catalyst as a fine powder. CVO was produced from rapeseed oil [4].

Methods

The experiments were all performed using an autoclave (type 4576A, Parr Instruments, Moline, IL, USA) at 380 °C, 50 bar H_2 pressure and with the gas entrainment impeller running at 1100 RPM. In previous investigations, these process conditions were found to be optimal for the catalytic HDO of CVO [5, 7]. The piping and instrumentation diagram of the test plant is presented in Fig. 1.

11 experiments were performed in total (Table 2). The experiments included the following:

- Continuous liquid-phase DO via catalytic HDO of CVO.
- Continuous investigations of gas residence time behaviour of the test plant.
- Batch experiments for the characterisation of GPRs.
- Batch investigations of gas phase inhomogeneity.

For the continuous catalytic HDO of CVO, H_2 and CVO were fed continuously into the process. The operation mode of the pilot plant is termed reactive stripping and was derived from the reactive distillation mode in the production process of CVO [4]. The reactor was mounted, rendered inert and finally CVO was provided in the reactor to give a filling level of two-thirds at the reaction temperature relative to the overall reactor volume. H_2 acts as a stripping and hydrogenation gas. The H_2 flow was set to 2.5 g/h by means of a mass flow counter (type M 12202139A, Bronkhorst High-Tech B.V., Ruurlo, Netherlands). Comparable investigations used a similar flow for H_2 [13, 30]. The liquid feed rate was 3.5 g/h and was chosen according to the preliminary investigations in semi-continuous mode [7]. Condensate samples were released continuously every 30 min at the beginning and then every 60 min after approximately 3 h time on stream (condensate fraction). The sump fraction was collected in the reactor. The catalytic HDO of CVO was run continuously investigating time on stream between 7 and 12 h. The preparation of all continuous catalytic HDO experiments was identical to assure reproducibility.

Continuous discharge of gas (CO and CO_2, CO_x in the following) was calculated according to Eq. (8) based on measurement data of the nondispersive infrared photometer.

$$m_{CO_x} = \sum_j \dot{V}_{\mathrm{ges},\Delta t,j} \times \overline{\rho_{CO_x,\Delta t,j}} \times (t_{j+1} - t_j) \times \frac{(v_j + v_{j+1})}{2}. \quad (8)$$

Volume fractions ($v_j + v_{j+1}$) measured by a nondispersive infrared photometer in each time interval ($t_{j+1} - t_j$), the total gas volume flow ($\dot{V}_{\mathrm{ges},\Delta t,j}$) and density of CO_x ($\overline{\rho_{CO_x,\Delta t,j}}$) were required parameters for the calculation.

The molar ratio of decarbonylation/decarboxylation alkane products (dec) versus the hydrodeoxygenation alkane products (hyd) is calculated according to Eq. (9):

$$\frac{\mathrm{dec}}{\mathrm{hyd}} = \frac{\sum_i \Delta n_{i,C_{n-1}}}{\sum_i \Delta n_{i,C_n}}, \quad (9)$$

where $\frac{\mathrm{dec}}{\mathrm{hyd}}$ molar ratio of produced C_n- and C_{n-1}-alkanes, $\Delta n_{i,C_{n-1}}$ net molar production of $C_{n\text{-}1}$-alkanes (C_8, C_9, C_{15}, C_{17}) (mol), $\Delta n_{i,C_n}$ net molar production of C_n-alkanes (C_9, C_{10}, C_{16}, C_{18}) (mol).

The net molar production of the respective alkanes was taken from GC/MS/FID analysis. The selection for alkanes (C_8, C_9, C_{10}, C_{15}, C_{16}, C_{17} and C_{18}) is related to chain length of the respective main fatty acids (C_9, C_{10}, C_{16}, C_{18}) in the CVO. These four selected fatty acids were found in concentrations ≥ 1.5 wt % in CVO and decomposed totally during HDO. The decomposition of these fatty acids can result in unchanged chain length alkanes, so called

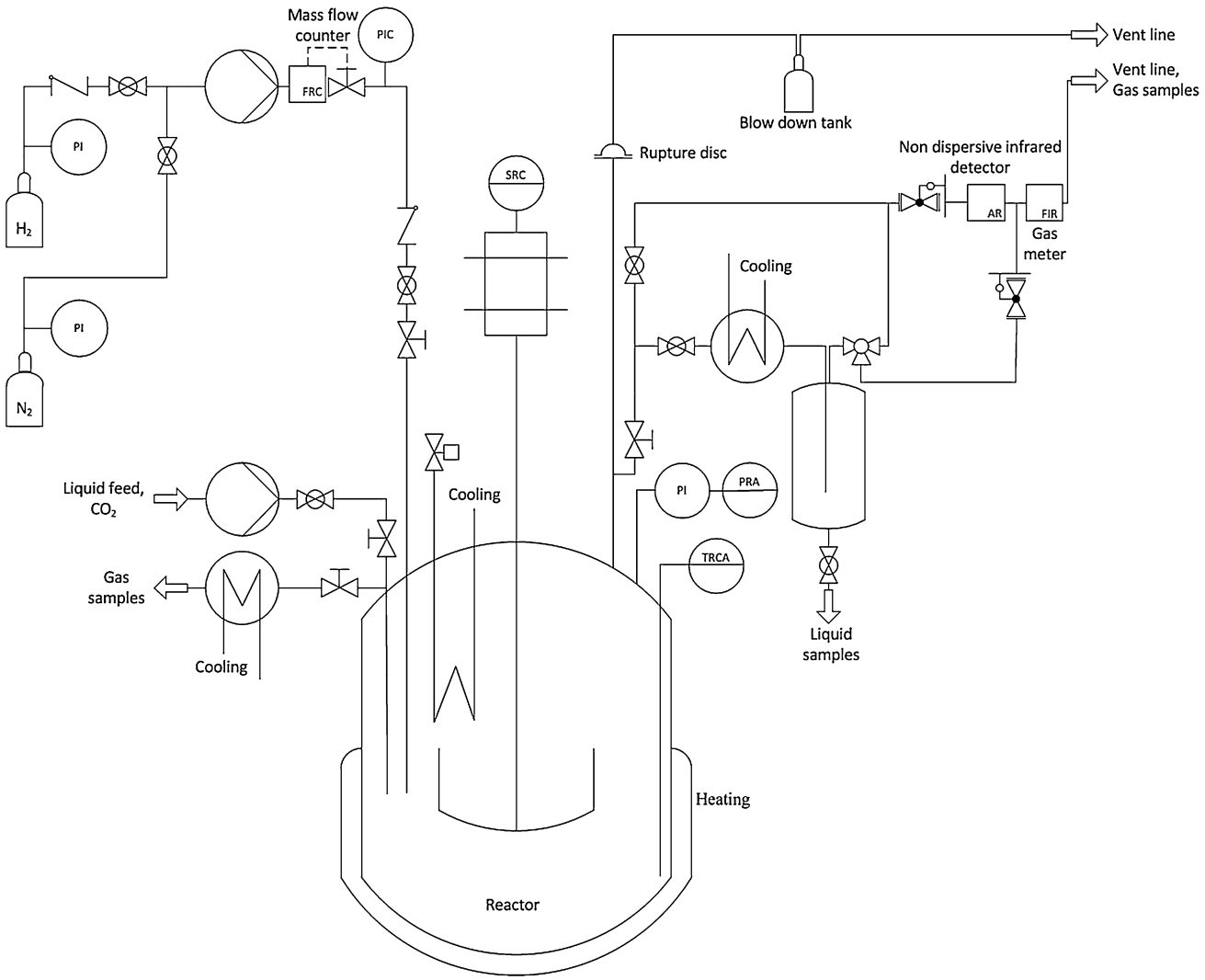

Fig. 1 Piping and instrumentation diagram of the test plant. Acronyms according to [29]: *A* alarm, *C* control, *F* flow, *I* indication, *P* pressure, *R* record, *S* speed, *T* temperature

Table 2 Overview of the performed experiments (380 °C, 50 bar H_2)

No.	Type of experiment
1, 2	Continuous HDO of CVO with CoMo catalyst
3–5	Continuous HDO of CVO with Pt catalyst
6, 7	Continuous gas residence time behaviour via pulsed tagging
8	Batch investigation of GPRs (CoMo catalyst)
9	Batch investigation of GPRs (Pt catalyst)
10, 11	Batch investigation of inhomogeneity effect

C_n-alkanes (C_9, C_{10}, C_{16}, C_{18}) via hydrogenation (reduction). The second possibility of decomposition is the chain length reduction by one carbon, resulting in the so-called C_{n-1}-alkanes (C_8, C_9, C_{15} and C_{17}) via decarbonylation and decarboxylation. The procedure of using molar product ratios for the characterisation of possible reactions was used in other studies before [13, 31–33].

For the continuous gas residence time studies, the same constant flow of H_2 was used as in continuous HDO experiments for the purpose of comparison (2.5 g/h). CO_2 was injected for pulsed tagging, once the reaction temperature was reached by means of a Teledyne Isco high-pressure pump (type 500 HP, Lincoln, NE, USA) via the liquid feed inlet. Two setups were investigated: one without liquid filling the reactor and one with filling the reactor with an inert liquid medium (BP Energol CS-HB 220). The liquid level of the reactor was (according to the experiments for the catalytic HDO of CVO) two-thirds at the reaction temperature relative to the overall reactor volume. Regarding the gas residence time, the CO_2 pulse passed the test plant (Fig. 1) in the same way as the reaction gases formed in an experiment for the catalytic HDO of CVO

(experiment 1–5) as follows: it was injected in the reactor and passed the condenser and the settling vessel of the liquid samples before the gas concentration was measured by the nondispersive infrared photometer. For both experiments on the gas residence time, approximately the same amount of CO_2 was injected. The mean gas residence time was calculated considering CO_2 concentration over time using linear interpolation between the measurement points. The gas residence time investigations were performed without catalysts to avoid GPRs.

For the batch investigations of the catalyst's selectivity for GPRs, the reactor was operated in batch mode. The procedure of preparation was the same as for a continuous HDO experiment, but without liquid filling. The catalyst amount was the same as for an experiment for the catalytic HDO of CVO (0.91 g for $CoMo/Al_2O_3$, 0.48 g for Pt/C, Table 3). After filling with H_2, the reactor was heated to the reaction temperature (380 °C). The first sample of each experiment was taken before the CO_2 injection to obtain a comparison value. Afterwards, the reactor pressure was adjusted to 50 bar H_2, and CO_2 was injected for pulsed tagging. The gas entrainment impeller was run at 1100 RPM. The experiments with both the catalysts were performed with similar initial concentration of CO_2 to ensure the comparability of the results. Gas sampling intervals were 5 min after injection. Each sample was drawn directly from the reactor after cooling and expansion to ambient conditions. Six samples could be taken from the overall reactor volume. Samples were then prepared for the GC/FID analysis.

The inhomogeneity of the gas phase in the reactor was investigated in batch mode considering two different sampling locations, using the CO_2 concentration as an indicator. The CO_2 injection was performed once the reactor reached 380 °C. Sampling was performed approximately 5 min after the CO_2 injection. The first sampling location was on the top of the reactor (approximately 86 mm from the bottom), and the second sample was drawn via the dip tube (approximately 25 mm from the bottom). Both samples were taken simultaneously.

Analysis of liquid and gaseous products

Liquid samples

For the liquid sample analysis, a G1530A GC (Agilent Technologies, Santa Clara, CA, USA) coupled with a quadrupole MS (5972A HP 6890, Hewlett Packard, Palo Alto, CA, USA) and FID was used. The database of the National Institute of Standard and Technology was used for the component identification. A VF5-ms capillary column from Agilent Technologies was installed (60 m × 0.25 mm × 0.25 µm). Perylene ($C_{20}H_{12}$) and used as an internal standard to avoid overlapping with component peaks. The split ratio was set to 15:1. The initial temperature of the column was 45 °C (holding time 4 min), followed by a heating ramp of 3 °C/min until 320 °C was reached. The final column temperature was held for 20 min. The GC was run in a constant flow mode with helium as the carrier gas at 2 mL/min. The average flow velocity was 31 cm/s. The FID was run at 350 °C. Nitrogen was used as the makeup gas with a flow of 45 mL/min; the synthetic air flow was 450 mL/min, and the H_2 flow was 40 mL/min. MS and FID detector was used in tandem for best identification and quantification of the components. The process of sample preparation was reproducible. Linear fitted curves were used for the calculation of the quantity of each component in agreement with the procedure applied by Artigues et al. [34].

Continuous gas composition

A calibrated Infralyt 50 nondispersive infrared photometer (Saxon Corporation, Dessau-Roßlau, Germany) was used for the continuous gas analysis. The nondispersive infrared

Table 3 Results of the continuous HDO experiments at 380 °C and 50 bar H_2 performed with CVO and CoMo/Pt as catalysts

No.	Catalyst	Time on stream (h)	CVO (g)	SF[a] product (g)	CF[b] products (g)	CO_x[c] (g)	Balance[d] (wt %)	O[e] CVO (wt %)	O SF product (wt %)
1	$CoMo/Al_2O_3$	7	120.5	82.2	24.8	2.15	91	5.3	0.7
2		7	120.7	85.1	21.8	2.12	90		1.0
3	Pt/C	7.5	127.0	90.4	15.4	2.63	85		0.5
4		8	128.6	94.4	18.8	2.75	90		0.8
5		12	142.9	103.4	28.6	3.29	95		0.3

[a] Sump fraction

[b] Condensate fraction

[c] CO and CO_2 gas calculated according to Eq. (8)

[d] Relative to feed mass: (SF product + CF product + CO_x)/CVO

[e] Oxygen by elemental analysis as repeat determination

photometer was used for both the experiments of the catalytic HDO of CVO and the gas residence time investigations.

Batch gas samples

The compositions of the batch gas samples were quantified with GC/FID on an Agilent Technologies 6890 N (G1530 N) machine equipped with a CoraPlot Q capillary column (CP7554, 25 m length, 0.53 mm inner diameter and 20 µm film thickness). The split was set to 10:1. The carrier gas was helium, with a flow of 20 mL/min. The initial oven temperature was 50 °C. The first heating ramp was 20 °C/min until 95 °C was reached and held for 4 min. The final temperature was 100 °C, reached with a second heating ramp of 12 °C/min. The FID was run at 220 °C. The H_2 flow was 40 mL/min, the air flow was 400 mL/min and the nitrogen makeup flow was 12 mL/min. The components were assigned according to their retention time similarity. Calibration runs with different test gases were performed as repeat determinations. Linear fitted curves were used to calculate the quantity of each component.

The gas samples were additionally analysed on a calibrated micro gas chromatograph (GCM Micro Box I, SLS Micro Technology Corporation, Mainz-Kastel, Germany) to confirm the gas composition results. A HayeSepA packed column was used for the measurement by means of a thermal conductivity detector. Argon was used as a carrier gas at a pressure of 3.5 bar.

Results and discussion

Results and discussion are given in two main chapters in the following order:

Continuous processing

- Liquid-phase DO via catalytic HDO of CVO for upgrading raw material CVO and to identify possible reactions.
- Gas residence time behaviour of the test plant.

Batch experiments

- Characterisation of GPRs.
- Inhomogeneity effect.

11 experiments were performed in total. An overview of these experiments is given in Table 2.

Continuous processing

The results of the HDO experiments as well as the gas residence time behaviour of the test plant are given in this chapter.

Liquid-phase DO via Catalytic HDO of CVO

Table 3 gives the overall mass balances and oxygen content of CVO and main products (sump fraction) for five experiments of the continuous catalytic HDO of CVO with 3.5 g/h feed and 2.5 g/h H_2 mass flow. The rotational speed of the gas entrainment impeller was 1100 RPM.

As can be seen from Table 3, sump fraction is the main liquid product. This is due to the initial filling of the reactor with CVO. The highest DO of the sump fraction was observed with 12 h time on stream in experiment 5. The lowest oxygen concentration is confirmed by the highest mass of m_{CO_x} for experiment 5 within all experiments (1–5). The overall mass balance is rising from 85 to 95 wt % with an increase in time on stream if we compare the experiments 3, 4 and 5 with Pt/C catalyst.

The results of the gas phase composition (nondispersive infrared photometer) are shown in Figs. 2 and 3 for all five experiments. Starting at time zero (heating switched on), the heating period until reaching the target temperature (380 °C) was approximately 1 h (62–64 min).

CO was detected slightly before CO_2 in every experiment. As the decrease in CO concentration in experiment 5 from 0.5 to 0.4 vol % took place very slowly (approximately within 5 h), it may be expected that the process was close to steady state at point C. It can be seen in Figs. 2 and 3 that the main DO of the liquid phase takes place rapidly at the beginning of the experiment due to steep inclination of the gas concentrations. Main product's (sump fraction) oxygen content confirms high DO after time on stream with both the catalysts (Table 3). Possibly the CO and CO_2 concentrations result from the DO/HDO reactions decarboxylation and decarbonylation. Considering this assumption, it can be seen that the Pt catalyst was more selective for these DO/HDO reactions compared to the CoMo catalyst. This is in agreement with literature, as can be seen in Table 4.

A dec/hyd ratio of 1 indicates the presence of both decarbonylation/decarboxylation and hydrogenation to the same extent. This is the case for both experiments with the CoMo catalyst (experiment 1 and 2). The same dec/hyd ratios of these experiments confirm reproducibility. Pt catalysts give clearly higher dec/hyd ratios than CoMo catalysts using vegetable oils as feedstocks. This effect is still visible in the HDO of CVO in this work. The lower dec/hyd ratio for CVO compared to the other results with Pt catalyst is due to the strongly reduced oxygen content of the CVO [36, 37]. This means, that the main part of decarbonylation/decarboxylation already occurred in the previous CVO production step [4]. In general, higher CO_x-yields should go along with increasing dec/hyd

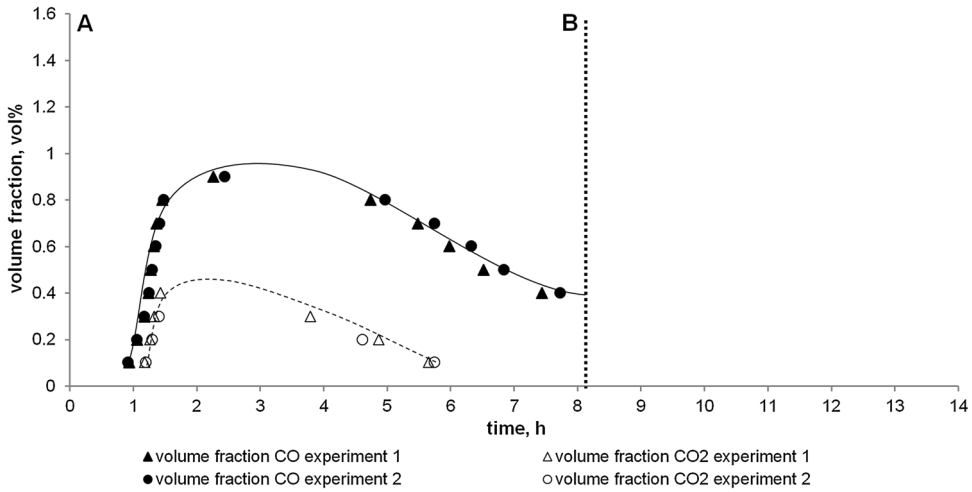

Fig. 2 Concentrations of CO and CO_2 during HDO at 380 °C and 50 bar H_2 with CoMo catalyst, *A* heating switched on, *B* heating switched off

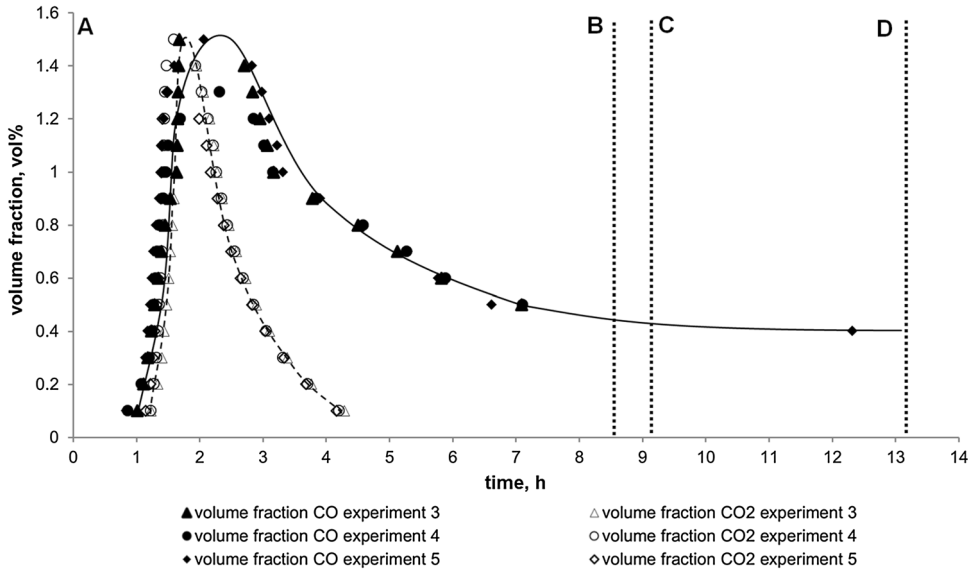

Fig. 3 Concentrations of CO and CO_2 during time on stream for the HDO experiments at 380 °C and 50 bar H_2 with Pt catalyst, *A* heating switched on, *B* heating switched off for experiment 3, *C* for experiment 4, *D* for experiment 5

ratios. This is confirmed by the data of this work given in Table 4.

Due to the higher concentration of CO compared to CO_2, both catalysts seem to be more selective for decarbonylation over decarboxylation. However, it is possible that the CO_2 is continuously decomposed to CO via GPRs during the HDO of CVO as well. CH_4 and C_2H_6 were measured only batch-wise every 30 min by micro gas chromatography. The maximum values for the CoMo catalyst (experiment 1) were 0.13 vol % for CH_4 and C_2H_6, and for the Pt catalyst (experiment 3) 0.16 vol % for CH_4 and 0.30 vol % for C_2H_6 were reached.

Due to the gas phase composition observed (mainly H_2, CO and CO_2), GPRs may occur (Eqs. 1–3). The gas concentrations (Figs. 2, 3) are compared to gas residence time behaviour of the plant to identify reaction time of main DO/HDO.

Gas residence time behaviour of the test plant

The gas residence time behaviour of the plant was investigated with and without filling the reactor with an inert liquid medium. Two experiments (6, 7) were performed. CO_2 pulsed tagging was applied for these investigations. Figure 4 shows the results of the CO_2 concentration plotted over time measured via a nondispersive infrared photometer.

Mean gas residence time for experiment 6 (B) and for experiment 7 (C) is shown. Downtime (A) of both the experiments was 26 min. As can be seen in Fig. 4, the downtime of both experiments was 26 min. It is defined as the time period between the pulse injection and the first detection of the gas by the nondispersive infrared photometer. Taking the downtime into account, the starting time of the DO during the catalytic HDO of CVO

Table 4 Product ratios (dec/hyd) from different model compounds resulting from DO/HDO reactions under a H_2 atmosphere using CoMo and Pt catalysts

	Feed	Catalyst	Reactor configuration	T (°C)	p (bar_{H2})	H_2/oil ratio (mol %/mol %)	Reaction time (h)	dec/hyd[a] (mol/mol)	Alkanes[b] dec/hyd	CO_x[c]	References
1	CVO	$CoMo/Al_2O_3$	Continuous reactive stripping	380	50	2.5 g_{H_2}/3.5 g_{CVO}	7	1.04	(C_8 + C_9 + C_{15} + C_{17})/(C_9 + C_{10} + C_{16} + C_{18})	2.15	This work
		$CoMo/Al_2O_3$		380	50	2.5 g_{H_2}/3.5 g_{CVO}	7	1.04		2.12	
		Pt/C		380	50	2.5 g_{H_2}/3.5 g_{CVO}	7.5	1.64		2.41	
		Pt/C		380	50	2.5 g_{H_2}/3.5 g_{CVO}	8	1.74		2.46	
		Pt/C		380	50	2.5 g_{H_2}/3.5 g_{CVO}	12	1.70		2.48	
2	Rapeseed oil	$CoMoS_2/Al_2O_3$	Continuous fixed bed, WHSV[d] = 1.5 h^{-1} (OMA, MCM), WHSV = 2 h^{-1} (Al_2O_3)	310	70	100	≥6	0.25	C_{17}/C_{18}		Kubička et al. [35]
		$CoMoS_2$/MCM-41		310	70	100	≥6	0.59			
		$CoMoS_2$/OMA1		310	70	100	≥6	0.18			
		$CoMoS_2$/OMA2		310	70	100	≥6	0.07			
3	Rapeseed oil	$CoMoS_2$/MCM-41	Continuous fixed bed, WHSV = 1.5 h^{-1}	320	23	50	≥6	1.32	C_{17}/C_{18}		Kubička et al. [33]
		$CoMoS_2$/MCM-41		320	55	50	≥6	0.40			
		$CoMoS_2$/MCM-41		320	110	50	≥6	0.15			
4	Sunflower oil	$CoMo/Al_2O_3$ (CoO (2.9 %), MoO3 (13.5 %))	Continuous flow reactor, LHSV[e] = 1 h^{-1}	380	20	600 (vol/vol)	Confirmation of the results in a 400 h experiment	0.34	C_{17}/C_{18}		Krár et al. [31]
				380	40	600 (vol/vol)		0.19			
				380	60	600 (vol/vol)		0.14			
				380	80	600 (vol/vol)		0.12			
5	Jatropha oil	$PtPd/\gamma$-Al_2O_3 (2 wt % Pt, 10 wt % Pd)	Continuous fixed bed, WHSV = 2 h^{-1}	350	30	600 (vol/vol)	5	58.99	C_{17}/C_{18}		Gong et al. [36]
6	Soybean oil	$CoMoS_x/Al_2O_3$ (Co (2.8 wt %), Mo (7.6 wt %))	Continuous fixed bed reactor (0.15 L), LHSV = 0.5 h^{-1}	300	50	30.1	3	0.46	C_{17}/C_{18}		Kim et al. [32]
				300	50	46.3	3	0.44			
				300	100	46.3	3	0.40			
				300	150	46.3	3	0.36			
				350	150	46.3	3	0.43			
				400	150	46.3	3	0.56			
				440	150	46.3	3	0.58			
		$CoMoS_x/Al_2O_3$ (Co (2.8 wt %), Mo (7.6 wt %))	Batch (0.109 L autoclave)	400	25		≥1	4.12	C_{17}/C_{18}		
				400	45		≥1	4.67			
				400	67		≥1	3.95			
				400	120		≥1	1.43			
				300	92		≥1	0.96			
				350	92		≥1	1.17			
				400	92		≥1	1.69			
				440	92		≥1	2.07			

Table 4 continued

	Feed	Catalyst	Reactor configuration	T (°C)	p (bar_{H2})	H_2/oil ratio (mol %/mol %)	Reaction time (h)	dec/hyd[a] (mol/mol)	Alkanes[b] dec/hyd	CO_x[c]	References
7	Tripalmitin in tetradecane	Pt/Al_2O_3 (5 wt % Pt)	Batch (0.05 L autoclave)	325	20		5	15.00	C_{15}/C_{16}		Madsen et al. [37]
	Oleic acid in tetradecane	Pt/Al_2O_3 (5 wt % Pt)		325	20		5	19.00	C_{17}/C_{18}		

[a] Molar ratio of alkanes based on total reaction time standardised to 100 %, independent of conversion degree for comparison [according to Eq. (9) for this work]

[b] Alkanes used to calculate dec/hyd

[c] Sum of CO_x within 7 h according to Eq. (8)

[d] Weight hourly space velocity

[e] Liquid hourly space velocity

(experiments 1–5) is approximately 26 min before the first detection of CO. This result highlights the importance of downtime/residence time characteristics to be considered; especially for the discussion of reaction temperature in conjunction with reaction time. The steep inclination of the CO_2 concentrations is in agreement with the gas concentrations observed during HDO of CVO (Figs. 2, 3). This confirms the fast DO/HDO of the main liquid product at the beginning of a HDO experiment (1–5). Regarding Figs. 2 and 3, the first detection of CO is close to the time needed to reach the target temperature of 380 °C. Taking downtime into account, this means that the formation of CO begins approximately 26 min earlier during the heating period. As a result, this indicates for experiments 1–5 that the starting temperature for DO/HDO via CO release is ≥230 °C. The formation of CO_2 began at approximately 365–375 °C in all five experiments (1–5). Successful HDO with Pt/C at a similar temperature (250 °C) was reported elsewhere [20]. Partly HDO of rapeseed oil with CoMO catalyst at 200 °C was reported from Pinto et al. [38]. HDO processes in this temperature range (≤250 °C) are often called mild HDO [20, 39].

Experiment 7, with an inert liquid filling, showed a higher maximum CO_2 concentration but the same downtime as experiment 6, without liquid filling. This may be due to both a higher concentration of CO_2, caused by the smaller gas volume in the reactor due to the liquid filling and the higher amount of injected CO_2, caused by the limited setting accuracy of the high-pressure pump. According to Fig. 4, the injected quantity of CO_2 and/or the filling of the reactor with an inert liquid media influenced the mean gas residence time slightly. Mean gas residence time was evaluated by linear interpolation between the measurement points. The mean gas residence time was 42 min for experiment 6 and 45 min for experiment 7.

Batch experiments

Characterisation of gas phase reactions

GPRs (1–3) may be responsible for the rapidly decreasing CO_2 concentration in the gas phase (Figs. 2, 3). For this reason, the selectivity of these chemical reactions was investigated with both the catalysts in experiments 8 and 9. After the CO_2 injection, six gas samples were taken from the reactor in each experiment (Fig. 1). The development of the reactor pressure during sampling in experiments 8 and 9 is shown in Fig. 5.

As can be seen in Fig. 5, the reactor pressure was constant between each gas sampling in the experiment with the CoMo catalyst (experiment 8), but it increased in the experiment with the Pt catalyst. It is assumed that this

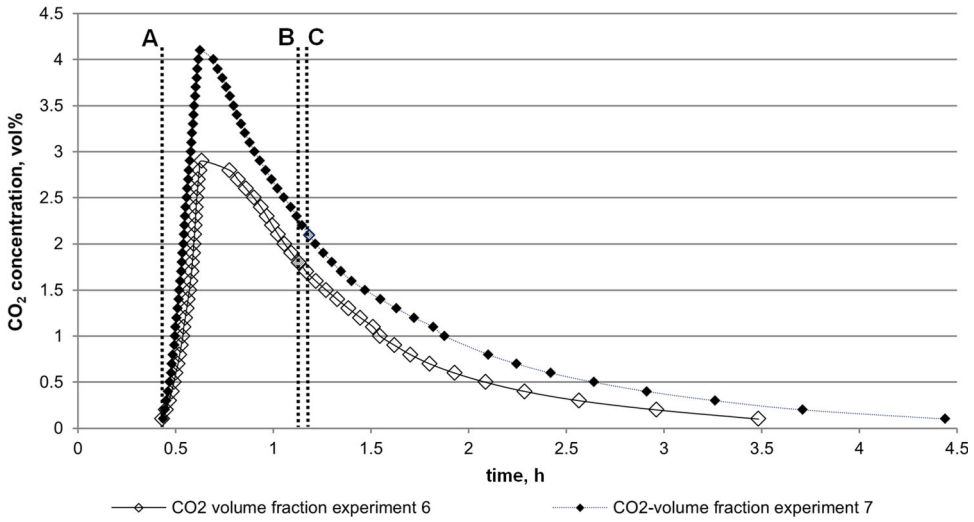

Fig. 4 Gas residence time behaviour of the test plant at 380 °C and 50 bar H_2 (1100 RPM, 2.5 g_{H_2}/h)

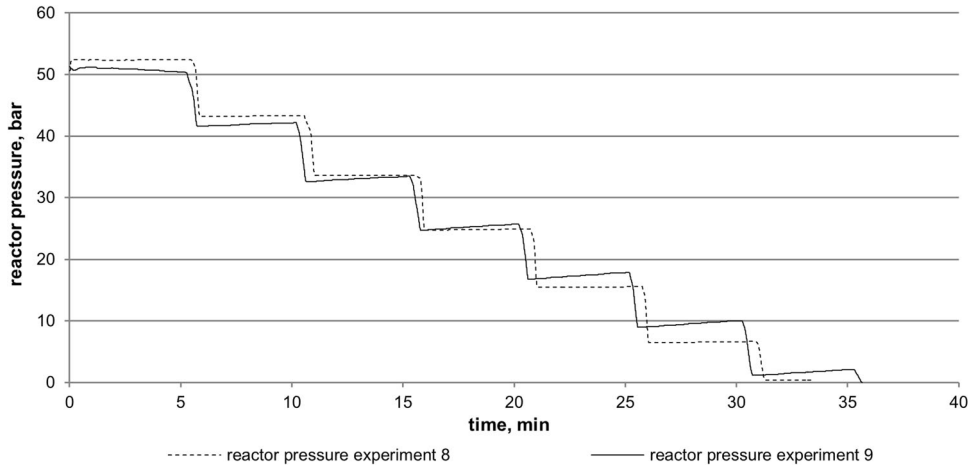

Fig. 5 Development of inner reactor pressure during the investigation of the GPRs without liquid filling at 380 °C, 50 bar. Experiment 8: CoMo catalyst, experiment 9: Pt catalyst

finding is due to the adsorption/desorption effects on the support of the catalyst (active carbon). Each stage in the diagram indicates a gas sample. Gas samples were removed until the reactor was evacuated. The adsorption/desorption of H_2 on Pt catalyst on active carbon (5 wt % Pt, BET = 650 m^2/g) was observed as well by Wang and Yang [40] (6 wt % Pt, BET = 3126 m^2/g). These authors showed a higher adsorption capacity of metal-doped carbon than that of plain carbon. At 50 bar and 298 K, the amount of H_2 adsorbed on Pt/carbon was found to be approximately 0.75 wt %, related to the mass of the catalyst [40]. The adsorbed amount depends on the reaction time, temperature and BET surface area.

Results from GC/FID analysis of the gas sample composition in experiments 8 and 9 are shown in Figs. 6 and 7.

Experiments 8 and 9 showed a remarkable CO_2 gas phase conversion due to CO and CH_4 generation. CO_2 conversion was obviously supported to a higher extend with the Pt catalyst compared to the CoMo catalyst. The detection of CO was unexpected, as the equilibrium constant for the CO-methanation reaction (2) according to Eq. (7) is 6×10^4 bar^{-2}, indicating the complete reaction of CO to CH_4. A possible explanation is the kinetic inhibition of the CO-methanation (2). A further unexpected observation in Fig. 7 is the initial concentration of CH_4 above zero (0.22 vol %) prior to the injection of CO_2. A reason could be that the CH_4 was generated by Pt supported reaction of the active carbon carrier material and the H_2 atmosphere during the heating phase (approximately 50 min).

Based on the results shown in Figs. 6 and 7, the quantity of each component was calculated according to ideal gas law, and the results are summarised in Table 5.

Higher hydrocarbons were not considered due to their very low concentrations ($\leq$0.11 vol %) during the entire experiments. The total carbon discharge in the collected gas samples was used to calculate the initial concentration of the CO_2 in the reactor, as given in Table 5 and marked

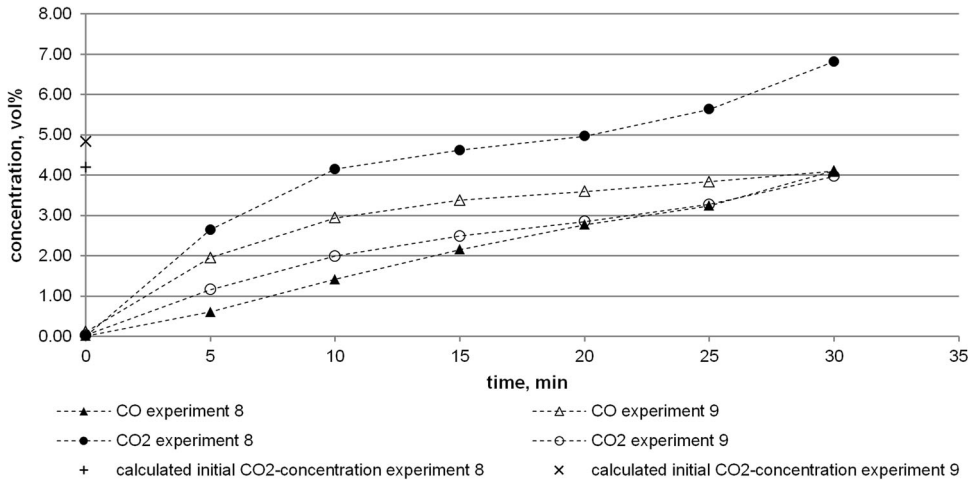

Fig. 6 CO and CO_2 concentration from experiment 8 (CoMo) and experiment 9 (Pt) at 380 °C and 50 bar. Sample time: 5 min after CO_2 injection at time zero (then 5 min intervals)

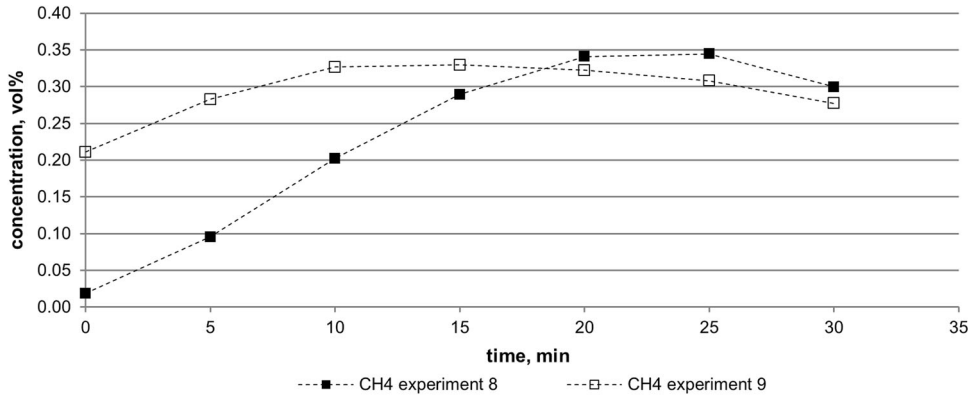

Fig. 7 CH_4 concentration in the gas samples of experiment 8 (CoMo) and experiment 9 (Pt) at 380 °C and 50 bar

Table 5 Quantity of each component from experiments 8 and 9 based on ideal gas law calculations

	CO_2		CO		CH_4		CO_2 initial concentration		
	g	mol	g	mol	g	mol	g	mol	vol %
Experiment 8	0.285	0.0065	0.0914	0.0033	0.0061	0.0004	0.445	0.0101	4.2
Experiment 9	0.213	0.0048	0.171	0.0061	0.0091	0.0006	0.506	0.0115	4.8

on the ordinate in Fig. 6. In the two experiments, the injected quantity of CO_2 was nearly the same. The experimental procedure was reproducible and the initial CO_2 concentrations were comparable in both experiments (8 and 9).

With these experimental data and the equilibrium constant calculated before the theoretical maximum partial pressure of CO (p_{CO}) at RWGS's equilibrium without subsequent methanation was calculated according to Eq. (10).

$$K_{p,(1)} = \frac{p_{CO} \cdot p_{H_2O}}{p_{CO_2} \cdot p_{H_2}} = \frac{p_{CO}^2}{\left(p_{0,CO_2} - p_{CO}\right) \cdot p_{H_2}}, \quad (10)$$

where $K_{p,(1)}$ equilibrium constant for RWGS (1), p_{CO} equilibrium partial pressure CO (bar), p_{H_2O} equilibrium partial pressure H_2O (bar), p_{CO_2} equilibrium partial pressure CO_2 (bar), p_{H_2} equilibrium partial pressure H_2 (bar), p_{0,CO_2} initial partial pressure CO_2 (bar).

Disregarding subsequent reactions of CO, partial pressures for equilibrium of RWGS were defined as follows: $p_{CO} = p_{H_2O}$ and $p_{CO_2} = p_{0,CO_2} - p_{CO}$.

The initial partial pressure of $CO_2 (p_{0,CO_2})$ in Eq. (10) was calculated from the total initial reactor pressure multiplied by the experimental initial CO_2 concentration, as given in Table 5. The equilibrium partial pressure of $H_2 (p_{H_2})$ was set equal to the difference between the measured initial reactor pressure after injection of CO_2 and the calculated p_{0,CO_2} by approximation. Based on these preconditions, the equilibrium partial pressure of CO (p_{CO}) was calculated from Eq. (10). Results are given in Table 6.

The results from Table 6 show that p_{CO_2} must be lower at RWGS's equilibrium compared to p_{CO}. Based on the

Table 6 Theoretical maximum partial pressure of CO based on equilibrium of Eq. (1) calculated from Eq. (10)

	Initial reactor pressure (bar)	CO_2 initial partial pressure, p_{0,CO_2} (bar)	H_2 equilibrium partial pressure, p_{H_2} (bar)	CO maximum partial pressure, p_{CO} (bar)	CO_2 maximum partial pressure, p_{CO_2} (bar)
Experiment 8	52.4	2.20	50.2	1.53	0.665
Experiment 9	51.5	2.49	49.0	1.68	0.814

Table 7 Theoretical maximum yields of CO and H_2O based on equilibrium of RWGS (1)

	Theoretical maximum yield of CO		Theoretical maximum yield of H_2O	
	g	mol	g	mol
Experiment 8	0.198	0.0071	0.127	0.0071
Experiment 9	0.217	0.0077	0.139	0.0077

data from Table 6 theoretical maximum yields of CO/H_2O from RWGS at equilibrium can be calculated via p_{CO} and ideal gas law, as one mole of CO results in one mole of H_2O: $n_{CO} = n_{H_2O} = p_{CO} \cdot V_{Reactor}/R \cdot T_{Reactor}$. By molar mass ($m_{H_2O} = n_{H_2O}/M_{H_2O}$), H_2O yields were calculated. The theoretical maximum yields of CO and H_2O are given in Table 7.

The experimental CO-yields of experiments 8 and 9 according to Table 6 are approximately 50 % below the theoretical maximum yields as shown in Table 7 and therefore within the expected theoretical limits. Presuming RWGS to occur, the formation of H_2O occurs in the same quantity compared to CO. The calculation of the H_2O-yields based on the experimental CO-yields for experiment 8 and 9 gave the following results:

- Experiment 8: m_{H_2O} = 0.06 g H_2O (M_{H_2O} · 0.0033 mol_{CO}).
- Experiment 9: m_{H_2O} = 0.11 g H_2O (M_{H_2O} · 0.0061 mol_{CO}).

These low mass yields of H_2O could not be detected. They probably disappeared by condensation in the gas samples. As expected, the theoretical maximum yields of H_2O were found to be higher than the calculated yields based on measurements. This can be seen when comparing the values from the experiments (8, 9) to the values given in Table 7.

Inhomogeneity effect

During the experimental investigations of the GPRs, an inhomogeneity of the gas phase was observed in the reactor. The first indicators could be detected in experiments 8 and 9, and the phenomenon is proven in experiments 10 and 11. This inhomogeneity effect made further kinetic investigations of GPRs impossible. However, the balance of the detected gas components could be analysed (Table 5).

The steady increase of CO and CO_2 shown in Fig. 6 gives the first indication of this inhomogeneity, which was caused due to density differences of the gases compared to H_2 (CO and CO_2 by factors 22 and 14, respectively). In the first gas sample, H_2 was predominantly removed, but in the last sample, the CO and CO_2 could expand more in the reactor, thus gradually raising the local concentration at the measuring point for each sample. The indication of inhomogeneity in experiments 8 and 9 can be derived from the fact that the measured CO_2 concentrations in the gas samples exceed the initial CO_2 concentration at the end of each investigation (Fig. 6), despite the CO_2 decomposition. Remarkably, this inhomogeneity effect occurred even though the gas entrainment impeller was run at 1100 RPM and the reactor temperature was 380 °C.

The measuring points for the gas samples are indicated in Fig. 8 in a simplified true-scale drawing (experiments 8 and 9: sample dip tube, experiments 10 and 11: sample dip tube and on the top of the reactor).

For the practical validation of the inhomogeneity effect, experiments 10 and 11 were carried out without catalyst and liquid filling in the reactor, considering the two different measuring points in the reactor. The CO_2 concentrations of the samples were analysed via micro gas chromatography, and the results are given in Fig. 9.

Sampling was performed 5 min after the CO_2 injection in both experiments 10 and 11 (sample 1) as before (in experiment 8 and 9). Sample 2 in experiment 11 was drawn immediately after sample 1. The quantitative reproducibility is limited (comparing experiment 10 and experiment 11, sample 1), but the inhomogeneity effect is obvious in all samples: The CO_2 concentration is higher at the dip tube measuring point, close to the bottom of the reactor, despite simultaneous sampling. The increase in the CO_2 concentration with the decreasing reactor pressure (comparing experiment 11, sample 1 and sample 2) is due to the expansion of the heavy gas phase.

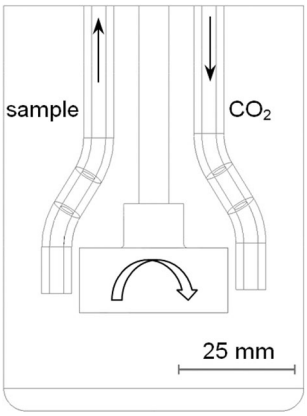

Fig. 8 True to scale drawing of the reactor interior; overall height approx. 86 mm, gas entrainment impeller and dip tubes for sampling

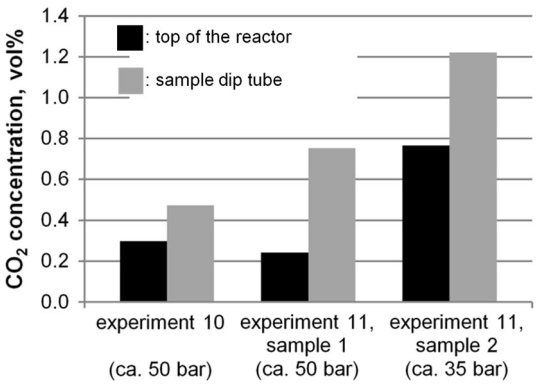

Fig. 9 CO_2 concentration at 380 °C and 50 bar in H_2 atmosphere in the reactor, comparing two measuring points [top of the reactor (*black bar*), sample dip tube (*grey bar*)]

Conclusions

Continuous experiments for the HDO of CVO were performed using an autoclave in a reactive stripping process. Used catalysts (Pt, CoMo) were suitable for this process due to high DO of the main product (sump fraction, Table 3). The main reaction gases were found to be CO_2 and CO, while the latter showed a higher concentration. Dec/hyd ratios were determined based on liquid phase composition. These calculated ratios correlate with the CO_x-yields calculated from the gas phase composition. The selectivity for DO/HDO via decarboxylation/decarbonylation is indicated by the dec/hyd ratio and was higher with the Pt catalyst compared to the CoMo catalyst.

To investigate whether the RWGS reaction (1) occurs, batch experiments for GPRs ($CO_2 + H_2$) were performed without CVO, using the same catalysts as in the continuous HDO experiments (CoMo, Pt). In these batch experiments, CO was found to be a product gas, indicating that the RWGS reaction occurs under the applied experimental conditions (380 °C, ca. 50 bar H_2 and ca. 2 bar CO_2). Additionally, CH_4 was found, indicating that methanation (2–3) occurs as well.

Thermodynamic data showed that RWGS is endergonic and CO-methanation is strongly exergonic under the applied conditions. Due to that, low RWGS yields and high CO-methanation yields are expected. Nevertheless, calculated RWGS yields based on equilibrium were found to be still significant due to H_2 excess. This was confirmed by GPR investigations with both catalysts. The experimental determined CO-yields were found to be within the theoretical limit. However, CO-methanation yields were found to be much lower than the expected according to low CH_4-concentrations from GPR investigations. This indicates kinetic inhibition. Further kinetic evaluations of RWGS and CO-methanation reactions (1–2) were not possible due to an unexpected inhomogeneity of the gas component concentrations in the reactor.

The enrichment in CO_2 and CO at the bottom of the reactor was clearly caused by the high density differences of the gas components CO_2, CO and CH_4 compared to H_2 (factors 22, 14 and 8, respectively), despite the elevated temperature and high RPM (380 °C, 1100 RPM).

Such inhomogeneity found in a common type reactor widely applied in research may cause similar problems in comparable investigations of other research groups. Nevertheless, this issue was not observed in the considered literature. CFD tools are to be applied as a tool for further clarification of this issue and to allow the confirmation of the unexpected experimental results shown in the present investigation.

Acknowledgments The present work is supported by a scholarship of the Hanns-Seidel-Stiftung by funds from the Federal Ministry of Education and Research, Germany. GC/MS/FID analyses were performed at the Thünen Institute of Wood Technology and Wood Biology, Hamburg, Germany.

Author contributions The manuscript was written through contributions of all authors. All authors have given approval to the final version of the manuscript and contributed equally.

Compliance with ethical standards

Conflict of interest The authors declare that they have no conflict of interest.

References

1. International Energy Agency: World Energy Outlook 2012. FRA, Paris (2012)
2. International Energy Agency World Energy Outlook: Executive Summary. FRA, Paris (2014). **2014**
3. Aatola, H., Larmi, M., Sarjovaara, T., Mikkonen, S.: Hydrotreated vegetable oil (HVO) as a renewable diesel fuel: trade-off between NOx, particulate emission, and fuel consumption of a heavy duty engine. SAE Int. J. Engines **1**(1), 1251–1262 (2009)
4. Augustin, C., Willner, T.: Investigation of vegetable oil conversion by thermal deoxygenation and cracking for alternative biofuel generation. In: Leal Filho, W., Mannke, F., Mohee, R., Schulte, V., Surroop, D. (eds.) Climate-Smart Technologies, pp. 563–576. Springer, Berlin (2013)
5. Sievers, A.: Hydroprocessing of cracked vegetable oil. Ph.D. thesis, University of the West of Scotland, Paisley, GB (2013)
6. Augustin, C.: Das Verhalten von Pflanzenölen bei der thermischen Zersetzung und der Desoxygenierung zu regenerativen Energieträgern. Dissertation, Helmut-Schmidt-Universität/Universität der Bundeswehr Hamburg, Hamburg, DE, Hamburg (2016)
7. Baldauf, E., Sievers, A., Willner, T.: In New developments in hydroprocessing of cracked vegetable oil. In: Hoffmann, C., Baxter, D., Maniatis, K., Grassi, A., Helm, P. (eds.) European Biomass Conference and Exhibition, 23–26 June 2014, ETA-Florence Renewable Energies, pp. 1034–1037 (2014)
8. Gosselink, R.W., Hollak, S.A.W., Chang, S.-W., van Haveren, J., de Jong, K.P., Bitter, J.H., van Es, D.S.: Reaction pathways for the deoxygenation of vegetable oils and related model compounds. ChemSusChem **6**, 1576–1594 (2013)
9. Jęczmionek, Ł., Porzycka-Semczuk, K.: Hydrodeoxygenation, decarboxylation and decarbonylation reactions while co-processing vegetable oils over NiMo hydrotreatment catalyst. Part II: thermal effects—experimental results. Fuel **128**, 296–301 (2014)
10. Chang, C.-C., Wan, S.-W.: China's motor fuels from tung oil. Ind. Eng. Chem. **39**, 1543–1548 (1947)
11. Madsen, A.T., Rozmysłowicz, B., Simakova, I.L., Kilpiö, T., Leino, A.-R., Kordás, K., Eränen, K., Mäki-Arvela, P., Murzin, D.Y.: Step changes and deactivation behavior in the continuous decarboxylation of stearic acid. Ind. Eng. Chem. Res. **50**(19), 11049–11058 (2011)
12. Gusmão, A., Brodzki, D., Djéga-Mariadassou, G., Frety, R.: Utilization of vegetable oils as an alternative source for diesel-type fuel: hydrocracking on reduced Ni/SiO2 and Sulphided Ni-Mo/γ-Al_2O_3. Catal. Today **5**, 533–544 (1989)
13. Endisch, M., Kuchling, T., Roscher, J.: Process balances of vegetable oil hydrogenation and coprocessing investigations with middle-distillates. Energy Fuels **27**, 2628–2636 (2013)
14. Jęczmionek, Ł., Porzycka-Semczuk, K.: Hydrodeoxygenation, decarboxylation and decarbonylation reactions while co-processing vegetable oils over a NiMo hydrotreatment catalyst. Part I: thermal effects—theoretical considerations. Fuel **131**, 1–5 (2014)
15. Snåre, M., Mäki-Arvela, P., Simakova, I., Myllyoja, J., Murzin, D.: Overview of catalytic methods for production of next generation biodiesel from natural oils and fats. Russ. J. Phys. Chem. B **3**(7), 1035–1043 (2009)
16. Kubátová, A., Luo, Y., Šťávová, J., Sadrameli, S.M., Aulich, T., Kozliak, E., Seames, W.: New path in the thermal cracking of triacylglycerols (canola and soybean oil). Fuel **90**(8), 2598–2608 (2011)
17. Wagman, D.D., Kilpatrick, J.E., Taylor, W.J., Pitzer, K.S., Rossini, F.D.: Heats free energies, and equilibrium constants of some reactions Involving O_2, H_2, H_2O, C, CO, CO_2, and CH4. J. Res. Natl. Bur. Stand. **34**, 143–161 (1945)
18. Snåre, M., Kubičková, I., Mäki-Arvela, P., Eränen, K., Murzin, D.Y.: Heterogeneous catalytic deoxygenation of stearic acid for production of biodiesel. Ind. Eng. Chem. Res. **45**(16), 5708–5715 (2006)
19. Lestari, S., Mäki-Arvela, P., Beltramini, J., Lu, G.Q.M., Murzin, D.Y.: Transforming triglycerides and fatty acids into biofuels. ChemSusChem **2**, 1109–1119 (2009)
20. Wildschut, J., Mahfud, F.H., Venderbosch, R.H., Heeres, H.J.: Hydrotreatment of fast pyrolysis oil using heterogeneous noble-metal catalysts. Ind. Eng. Chem. Res. **48**(23), 10324–10334 (2009)
21. Basu, P.: Combustion and Gasification in Fluidized Beds, p. 473. Taylor & Francis, Boca Raton (2006)
22. National Institute of Standards and Technology Thermodynamische Daten. http://webbook.nist.gov/chemistry/. Accessed 28 Aug 2015
23. Elvers, B.: Formamides and hexamethylenediamine. In: Elvers, B., Hawkins, S., Ravenscroft, M., Rounsaville, J.F., Schulz, G. (eds.) Ullmann's Encyclopedia of Industrial Chemistry, vol. A12, p. 632. Wiley-VCH, Weinheim (1989)
24. Fisk, C.A., Morgan, T., Ji, Y., Crocker, M., Crofcheck, C., Lewis, S.A.: Bio-oil upgrading over platinum catalysts using in situ generated hydrogen. Appl. Catal. A **358**(2), 150–156 (2009)
25. Şenol, Oİ., Viljava, T.R., Krause, A.O.I.: Hydrodeoxygenation of methyl esters on sulphided NiMo/γ-Al_2O_3 and CoMo/γ-Al_2O_3 catalysts. Catal. Today **100**(3–4), 331–335 (2005)
26. Cugini, A.V., Rothenberger, K.S., Ciocco, M.V., Veloski, G.V.: Comparison of hydrogenation and dehydrogenation behavior and coal conversion activity upon the addition of coal for supported and unsupported molybdenum catalysts. Energy Fuels **11**, 213–220 (1997)
27. Iida, H., Itoh, D., Minowa, S., Yanagisawa, A., Igarashi, A.: Hydrogenation of soybean oil over various platinum catalysts: effects of support materials on trans fatty acid levels. Catal. Commun. **62**, 1–5 (2015)
28. Hara, Y., Endou, K.: The drastic effect of platinum on carbon-supported ruthenium-tin catalysts used for hydrogenation reactions of carboxylic acids. Appl. Catal. A **239**, 181–195 (2003)
29. DIN EN 62424, Darstellung von Aufgaben der Prozessleittechnik—Fließbilder und Datenaustausch zwischen EDV-Werkzeugen zur Fließbilderstellung und CAE-Systemen. In: (IEC 65/544/CDV:2013). Beuth, Berlin, pp. 1–107 (2014)
30. Wang, C., Liu, Q., Song, J., Li, W., Li, P., Xu, R., Ma, H., Tian, Z.: High quality diesel-range alkanes production via a single-step hydrotreatment. Catal. Today **234**, 153–160 (2014)
31. Krár, M., Kovács, S., Kalló, D., Hancsók, J.: Fuel purpose hydrotreating of sunflower oil on CoMo/Al2O3 catalyst. Bioresour. Technol. **101**(23), 9287–9293 (2010)
32. Kim, S.K., Brand, S., Lee, H.-S., Kim, Y., Kim, J.: Production of renewable diesel by hydrotreatment of soybean oil: effect of reaction parameters. Chem. Eng. J. **228**, 114–123 (2013)
33. Kubička, D., Bejblová, M., Vlk, J.: Conversion of vegetable oils into hydrocarbons over CoMo/MCM-41 catalysts. Top. Catal. **53**, 168–178 (2010)
34. Artigues, A., Puy, N., Bartrolí, J., Fábregas, E.: Comparative assessment of internal standards for quantitative analysis of bio-oil compounds by gas chromatography/mass spectrometry using statistical criteria. Energy Fuels **28**(6), 3908–3915 (2014)
35. Kubička, D., Šimáček, P., Žilková, N.: Transformation of vegetable oils into hydrocarbons over mesoporous-alumina-supported CoMo catalysts. Top. Catal. **52**(1–2), 161–168 (2009)
36. Gong, S., Shinozaki, A., Shi, M., Qian, E.W.: Hydrotreating of jatropha oil over alumina based catalysts. Energy Fuels **26**(4), 2394–2399 (2012)
37. Madsen, A.T., Ahmed, E.H., Christensen, C.H., Fehrmann, R., Riisager, A.: Hydrodeoxygenation of waste fat for diesel

production: study on model feed with Pt/alumina catalyst. Fuel **90**(11), 3433–3438 (2011)
38. Pinto, F., Martins, S., Gonçalves, M., Costa, P., Gulyurtlu, I., Alves, A., Mendes, B.: Hydrogenation of rapeseed oil for production of liquid bio-chemicals. Appl. Energy **102**, 272–282 (2013)
39. Boscagli, C., Raffelt, K., Zevaco, T.A., Olbrich, W., Otto, T.N., Sauer, J., Grunwaldt, J.-D.: Mild hydrotreatment of the light fraction of fast-pyrolysis oil produced from straw over nickel-based catalysts. Biomass Bioenergy **83**, 525–538 (2015)
40. Wang, L., Yang, R.T.: Hydrogen storage properties of carbons doped with ruthenium, platinum, and nickel nanoparticles. J. Phys. Chem. **112**, 12486–12494 (2008)